Local Mesh Patterns Versus Local Binary Patterns: Biomedical Image Indexing and Retrieval

Subrahmanyam Murala and Q. M. Jonathan Wu, *Senior Member, IEEE*

***Abstract*—In this paper, a new image indexing and retrieval algorithm using local mesh patterns are proposed for biomedical image retrieval application. The standard local binary pattern encodes the relationship between the referenced pixel and its surrounding neighbors, whereas the proposed method encodes the relationship among the surrounding neighbors for a given referenced pixel in an image. The possible relationships among the surrounding neighbors are depending on the number of neighbors, P. In addition, the effectiveness of our algorithm is confirmed by combining it with the Gabor transform. To prove the effectiveness of our algorithm, three experiments have been carried out on three different biomedical image databases. Out of which two are meant for computer tomography (CT) and one for magnetic resonance (MR) image retrieval. It is further mentioned that the database considered for three experiments are OASIS-MRI database, NEMA-CT database, and VIA/I–ELCAP database which includes region of interest CT images. The results after being investigated show a significant improvement in terms of their evaluation measures as compared to LBP, LBP with Gabor transform, and other spatial and transform domain methods.**

***Index Terms*—Biomedical image retrieval (CBIR), Gabor transform (GT), local binary pattern (LBP), local mesh patterns (LMeP), texture.**

I. Introduction

A. Motivation

THERE has been a radical expansion of biomedical images in medical institutions and hospitals for patient diagnosis. Database for patient diagnosis exists in different formats such as computer tomography (CT), magnetic resonance imaging (MRI), ultrasound (US), X-ray, etc. However, one cannot make use of this data unless it is organized to allow efficient access, search, and retrieval. To address this problem, content-based biomedical image retrieval came into existence. The content-based image retrieval (CBIR) utilizes visual contents of an image such as *color, texture, shape, faces, spatial layout* etc., to represent and index the image database. The previously available biomedical image retrieval systems are presented in [1]–[6].

The feature extraction in CBIR is a prominent step whose effectiveness depends upon the method adopted for extracting features from given images. Comprehensive and extensive literature survey on CBIR is presented in [7]–[11].

The visual content descriptors are either global or local. A global descriptor represents the visual features of the whole image, whereas a local descriptor represents the visual features of regions or objects to describe the image. Furthermore, these are subdivided into two categories, spatial and transform domain-based features. The first approach makes use of pixels (or a group of adjacent pixels) gray value and the second approach makes use of transformed data of the gray image for feature extraction.

Texture-based biomedical image retrieval is a branch of texture analysis particularly well suited for the identification of disease region, and then retrieval of related documents in the database is making it a star attraction from medical perspective. Cai *et al.* [12] have used the physiological kinetic feature which reduces the image storage memory for positron emission tomography (PET) image retrieval. Scott and Shyu have designed the biomedical media retrieval system [1], where they utilize the entropy balanced statistical (EBS) k-d tree for feature extraction. The index utilizes statistical properties inherent in large-scale biomedical media databases for efficient and accurate searches. Rahman *et al.* [13] have designed the relevance feedback-based biomedical image retrieval system. They have proposed the query-specific adaptive linear combination of similarity-matching approach by relying on the image classification and feedback information from users. Nakayama *et al.* [14] investigated four objective similarity measures as an image retrieval tool for selecting lesions similar to unknown lesions on mammograms. Classification of benign and malignant breast masses based on shape and texture features in sonography images is proposed in [15]. The mass regions were extracted from the region of interest (ROI) subimage by implementing a hybrid segmentation approach based on level set algorithms. In [16], a boosting framework for visuality-preserving distance metric learning is proposed for medical image retrieval. The mammographic images and dataset from ImageCLEF are used for performance evaluation. Quellec *et al.* [17] proposed the optimized wavelet transform for medical image retrieval by adapting the wavelet basis, within the lifting scheme framework for wavelet decomposition. The weights are assigned between wavelet subbands. They used the diabetic retinopathy and mammographic databases for medical image retrieval. The wavelet transform-based brain image retrieval is presented in [18]. The cooccurrence matrix-based retrieval of medical CT and MRI images in different tissues is can be seen in [19]. Furthermore, the image retrieval of different body parts is proposed in [20], which employ color quantization and wavelet transform.

Manuscript received August 13, 2012; revised February 8, 2013 and June 21, 2013; accepted October 24, 2013. Date of publication November 4, 2013; date of current version May 1, 2014. This work was supported by the Canada Research Chair program, the Natural Sciences and Engineering Research Council of Canada (NSERC) Discovery Grant.

The authors are with the Computer Vision and Sensing Systems Lab, Department of Electrical and Computer Engineering, University of Windsor, Windsor, ON N9B 3P4, Canada (e-mail: muralasu@uwindsor.ca; jwu@uwindsor.ca).

Color versions of one or more of the figures in this paper are available online at http://ieeexplore.ieee.org.

Digital Object Identifier 10.1109/JBHI.2013.2288522

B. Related Work

The features, $k-d$ tree [1], cooccurrence matrix [19] etc., are computationally more expansive. To address this computational complexity, the local binary pattern (LBP) [21] is proposed. The LBP operator was introduced by Ojala *et al.* [21] for texture classification. Success in terms of speed (no need to tune any parameters) and performance is reported in many research areas such as texture classification [21]–[25], face recognition [26]–[28], object tracking [29], [30], image retrieval [31]–[37], and interest point detection [38]. Peng *et al.* proposed the texture feature extraction based on a uniformity estimation method in brightness and structure in chest CT images [35]. They used the extended rotational invariant LBP and the gradient orientation difference to represent brightness and structure in the image. Unay *et al.* proposed the local structure-based region-of-interest retrieval in brain MR images [36]. Quantitative analysis of pulmonary emphysema using LBP is presented in [37]. They improved the quantitative measures of emphysema in CT images of the lungs by using joint LBP and intensity histograms. Li and Meng have proposed the automatic recognition of tumor for wireless capsule endoscopy (WCE) images [39]. The candidate color texture feature that integrates uniform LBP and wavelet is proposed to characterize WCE images. Furthermore, the detection of bleeding regions for capsule endoscopy images using LBP is presented in [40]. Facial paralysis video retrieval system using LBP is proposed in [41]. The symmetry of facial movements is measured by the resistor-average distance between LBP features extracted from the two sides of the face. Support vector machine is applied to provide quantitative evaluation of facial paralysis.

C. Main Contribution

The pattern-based features available in the literature are encoding the relationship between the center pixel and its surrounding neighbors. This observation has motivated us to propose the local mesh pattern (LMeP), which encodes the relationship among the surrounding neighbors for a given center pixel in an image. In addition, the effectiveness of our algorithm is confirmed by combining it with Gabor transform. The performance of the proposed method is tested by conducting three experiments on three different biomedical databases.

The organization of the paper is as follows. In section I, a brief review of biomedical image retrieval and related work are given. Section II presents a concise review of local patterns (LBP and LMeP). Section III presents the concept of multiscale feature extraction, proposed system framework and the query matching. Experimental results and discussions are presented in Section IV and finally in Section V, we conclude with the summary of work.

II. Local Patterns

A. Local Binary Patterns

The LBP operator was introduced by Ojala *et al.* [16] for texture classification. Given a center pixel in the image, LBP value is computed by comparing its gray value with its neighbors

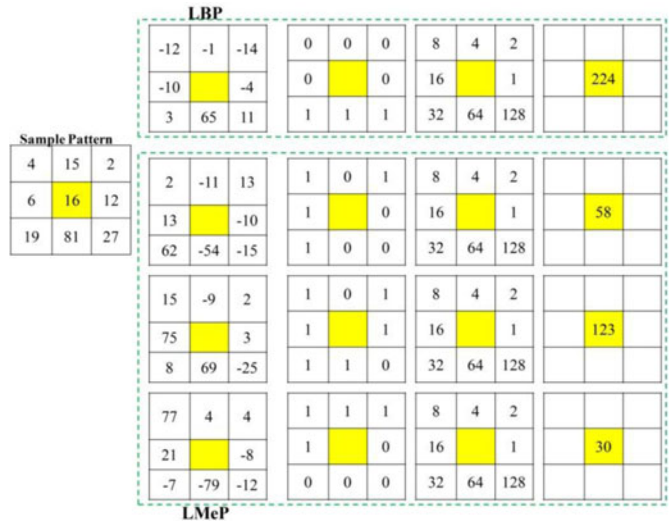

Fig. 1. Example of obtaining LBP and LMeP for the 3 × 3 pattern.

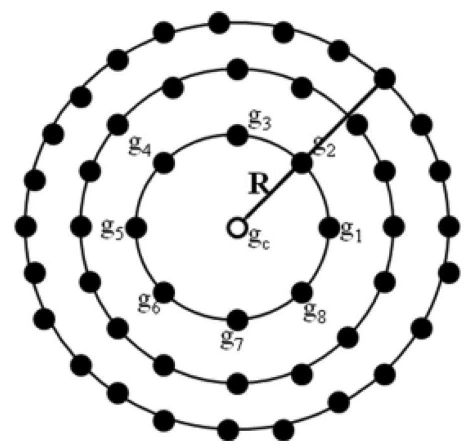

Fig. 2. Circular neighborhood sets for different (P, R).

as shown in Fig. 1, based on (1).

$$\mathrm{LBP}_{P,R} = \sum_{i=1}^{P} 2^{(i-1)} \times f_1(g_i|_R - g_c) \quad (1)$$

$$f_1(x) = \begin{cases} 1 & x \geq 0 \\ 0 & \text{else} \end{cases} \quad (2)$$

where g_c is the gray value of the center pixel, $g_i|_R$ is the gray value of neighbor at radius R from the center pixel (g_c), P is the number of neighbors at a distance (radius) R form the center pixel (g_c) in an image.

An examples of circular neighbor sets for different configurations of (P, R) can be seen in Fig. 2.

B. Local Mesh Patterns (LMeP)

The idea of the LBP has motivated us to propose the LMeP for biomedical image retrieval. The LMeP value is computed based on the relationship among the surrounding neighbors for a given center pixel in an image [see in (3)]. Fig. 1 illustrates

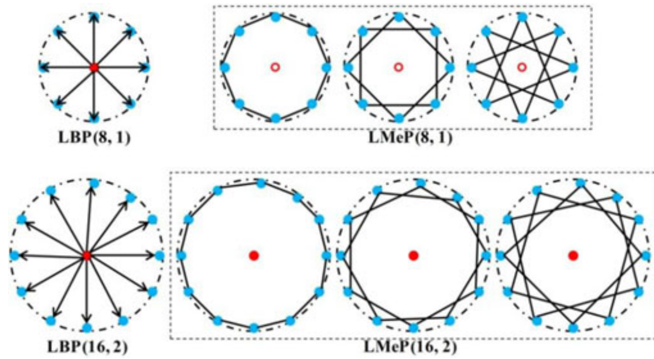

Fig. 3. LBP and the first three LMeP calculations for a given (*P, R*).

the LMeP values calculated for a given 3×3 pattern.

$$\mathrm{LMeP}^{j}_{P,R} = \sum_{i=1}^{P} 2^{(i-1)} \times f_1(g_\alpha|_R - g_i|_R)$$
$$\alpha = 1 + \mathrm{mod}((i+P+j-1), P)$$
$$\forall j = 1, 2, .., (P/2) \tag{3}$$

where j represents the LMeP index and mod (x, y) returns the reminder for x/y operation.

From (3), it can be observed that the possible LMeP patterns for P neighbors are P/2. In this paper, we consider only first three LMeP patterns [j = 1, 2, 3 in (3)] for experimentation as shown in Figs. 1 and 3. Fig. 3 illustrates the LBP and the first three LMeP calculations for a given (P, R). In this paper, (8,1), (16, 2) and (24, 3) combinations are considered for experimentation.

For the local pattern with P neighboring pixels, there are 2^P (0 to 2^P–1) possible values for both LBP and LMeP, resulting in a feature vector of length 2^P. A high computational cost is involved in extracting such a feature vector. Thus, uniform patterns [23] are considered to reduce the computational cost. A uniform pattern refers to a circular binary representation having limited discontinuities. In this paper, patterns with two or less discontinuities in the circular binary representation are termed as uniform, while rest of the patterns are termed as nonuniform. Thus, the distinct uniform patterns for a given query image would be $P(P-1)+2$. The possible uniform patterns for P = 8 can be seen in [23].

After identifying the local pattern, PTN (the LBP or the first three LMePs), the whole image is represented by building a histogram using (4)

$$H_S(l) = \frac{1}{N_1 \times N_2} \sum_{j=1}^{N_1} \sum_{k=1}^{N_2} f_2(\mathrm{PTN}(j,k), l);$$
$$l \in [0, P(P-1)+2] \tag{4}$$

$$f_2(x,y) = \begin{cases} 1 & \text{if } x = y \\ 0 & \text{else} \end{cases} \tag{5}$$

where $N_1 \times N_2$ represents the size of an input image.

Fig. 4 illustrates the feature maps obtained by applying the LBP and the first three LMePs operators on the referenced MR

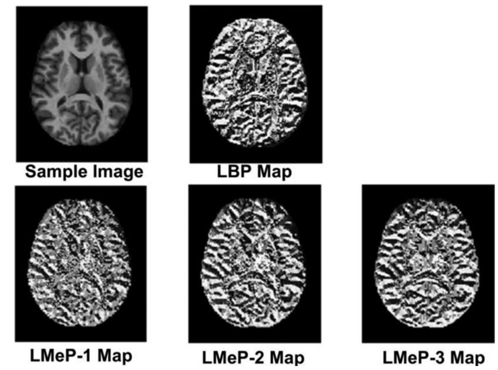

Fig. 4. Example of LBP and LMeP feature maps: sample image, LBP feature map, first LMeP feature map, second LMeP feature map and third LMeP feature map.

image. The experimental results demonstrate that the proposed LMeP shows better performance as compared to LBP, indicating that it can capture more edge information than LBP for biomedical image retrieval.

III. Multiscale Feature Extraction

In the literature, it is observed that the pattern-based features are analyzed by combining it with the Gabor transform. Hence, in this paper, we also confirm the effectiveness of our algorithm by combining it with Gabor transform (GT).

A. Gabor Transform

Subrahmanyam *et al.* [42] have given the spatial implementation of GT. A 2-D Gabor function is a Gaussian modulated by a complex sinusoid. It can be specified by the frequency of the sinusoid ω and the standard deviations σ_x and σ_y of the Gaussian envelope as follows:

$$\psi(x,y) = \frac{1}{2\pi\sigma_x\sigma_y} e^{[-(1/2)(x^2/\sigma_x^2 + y^2/\sigma_y^2) + 2\pi j\omega x]} \tag{6}$$

The Gabor wavelets are obtained by dilation and rotation of the generating function $\psi(x,y)$as follows:

$$\psi_{mn}(x,y) = a^{-m}\psi(x', y') \tag{7}$$
$$\text{where } x' = a^{-m}(x\cos\theta + y\sin\theta)$$
$$y' = a^{-m}(-x\sin\theta + y\cos\theta)$$
$$\theta = n\pi/K \tag{8}$$

where $m \in \{0, \ldots, S-1\}$ and $n \in \{0, \ldots, K-1\}$ represent scale and orientation, respectively; K and S are the number of desired orientations and scales, respectively.

The variables in the (6)–(8) are defined as follows:

$$a = (U_h/U_l)^{-1/s-1}, \ \omega_{m,n} = U_h \tag{9}$$

$$\sigma_{x,m,n} = \frac{(a+1)\sqrt{2\ln 2}}{2\pi a^m (a-1) U_l} \tag{10}$$

$$\sigma_{y,m,n} = \frac{1}{2\pi\tan\left(\frac{\pi}{2K}\right)\sqrt{\frac{U_h^2}{2\ln 2} - \left(\frac{1}{2\pi\sigma_{x,m,n}}\right)^2}} \tag{11}$$

where U_h and U_l are the upper and lower bound of the designing frequency band, respectively. In this implementation, we used the following constants as used in the literature: $U_l = 0.05$, $U_h = 0.49$.

The response of Gabor filter is the convolution of Gabor window with image *I,* and is given as

$$G_{mn}(x, y) = \sum_s \sum_t I((x - s, y - t)\psi^*_{\mathrm{mn}}(s, t). \quad (12)$$

B. Gabor Local Mesh Patterns (GLMeP)

In this paper, the real part of Gabor responses are utilized for GLMeP feature maps calculation. The performance of GLMeP is analyzed with *P*/2 directions and different scales (see in Section IV-A). From experiments, it is clear that three scales and *P*/2 directions of GT are showing better performance as compared to the other scales of GT.

For a given center pixel at (x, y), the GLMeP operators for $P = 8$ and $R = 1$ are calculated as follows:

$$\mathrm{GLMeP}^1_{P,R}\Big|_{P=8,R=1} = \left\{\begin{array}{c} f_1(G_{45^\circ}(x-R, y+R) - G_{0^\circ}(x, y+R)), \\ f_1(G_{90^\circ}(x-R, y) - G_{45^\circ}(x-R, y+R)) \\ f_1(G_{135^\circ}(x-R, y-R) - G_{90^\circ}(x-R, y)) \\ f_1(G_{0^\circ}(x, y-R) - G_{135^\circ}(x-R, y-R)) \\ f_1(G_{45^\circ}(x+R, y-R) - G_{0^\circ}(x, y-R)) \\ f_1(G_{90^\circ}(x+R, y) - G_{45^\circ}(x+R, y-R)) \\ f_1(G_{135^\circ}(x+R, y+R) - G_{90^\circ}(x+R, y)) \\ f_1(G_{0^\circ}(x, y+R) - G_{135^\circ}(x+R, y+R)) \end{array}\right\} \quad (13)$$

$$\mathrm{GLMeP}^2_{P,R}\Big|_{P=8,R=1} = \left\{\begin{array}{c} f_1(G_{90^\circ}(x-R, y) - G_{0^\circ}(x, y+R)), \\ f_1(G_{135^\circ}(x-R, y-R) - G_{45^\circ}(x-R, y+R)) \\ f_1(G_{0^\circ}(x, y-R) - G_{90^\circ}(x-R, y)) \\ f_1(G_{45^\circ}(x+R, y-R) - G_{135^\circ}(x-R, y-R)) \\ f_1(G_{90^\circ}(x+R, y) - G_{0^\circ}(x, y-R)) \\ f_1(G_{135^\circ}(x+R, y+R) - G_{45^\circ}(x+R, y-R)) \\ f_1(G_{0^\circ}(x, y+R) - G_{90^\circ}(x+R, y)) \\ f_1(G_{45^\circ}(x-R, y+R) - G_{135^\circ}(x+R, y+R)) \end{array}\right\} \quad (14)$$

$$\mathrm{GLMeP}^3_{P,R}\Big|_{P=8,R=1} = \left\{\begin{array}{c} f_1(G_{135^\circ}(x-R, y-R) - G_{0^\circ}(x, y+R)), \\ f_1(G_{0^\circ}(x, y-R) - G_{45^\circ}(x-R, y+R)) \\ f_1(G_{45^\circ}(x+R, y-R) - G_{90^\circ}(x-R, y)) \\ f_1(G_{90^\circ}(x+R, y) - G_{135^\circ}(x-R, y-R)) \\ f_1(G_{135^\circ}(x+R, y+R) - G_{0^\circ}(x, y-R)) \\ f_1(G_{0^\circ}(x, y+R) - G_{45^\circ}(x+R, y-R)) \\ f_1(G_{45^\circ}(x-R, y+R) - G_{90^\circ}(x+R, y)) \\ f_1(G_{90^\circ}(x-R, y) - G_{135^\circ}(x+R, y+R)) \end{array}\right\} \quad (15)$$

where $G_\alpha(x, y)$ is the response of GT in α direction.

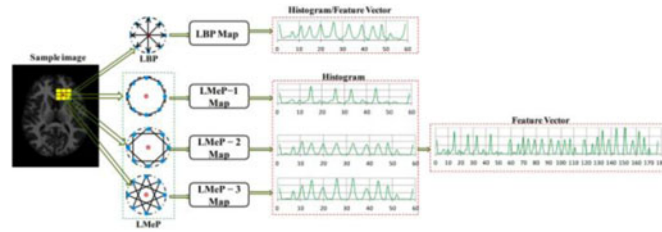

Fig. 5. Feature vector generation based on LBP and LMeP.

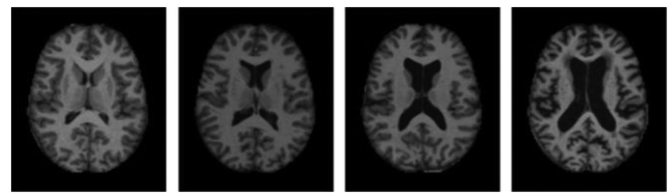

Fig. 6. Sample images from OASIS database (one image per category).

TABLE I
PERFORMANCE OF GLMEP WITH DIFFERENT SCALES OF GT IN TERMS OF ARP ON OASIS-MRI DATABASE

Method	Precision (%) (*n*=10)			
	One scale GT	Two scales GT	Three Scales GT	Four Scales GT
GLMePu2_8_1	41.80	54.53	56.34	52.12
GLMePu2_16_2	41.63	43.15	53.54	40.36
GLMePu2_24_3	41.42	40.71	52.54	45.21

Similarly, GLMePs are calculated for (16, 2) and (24, 3).

Eventually, the given image is converted to GLMeP images having values ranging from 0 to $P(P{-}1){+}2$ (for uniform two patterns). After calculation of GLMePs, the whole image is represented by building a histograms supported by (4).

C. Feature Extraction

Fig. 5 illustrates the feature extraction for the LBP and the proposed method (LMeP). The algorithm for LMeP is given as follows.

Algorithm: Input: Image; Output: Feature Vector

1) Load the gray scale image (if it is RGB, convert into gray scale).
2) Generate the first three LMeP operators for each center pixel.
3) Calculate the local differences among the neighbor pixels.
4) Calculate the binary patterns.
5) Construct the histograms based on uniform two patterns.
6) Form a feature vector by concatenating three histograms.

D. Similarity Measurement

The feature vector for query image Q represented as $f_Q = (f_{Q_1}, f_{Q_2}, \ldots, f_{Q_{Lg}})$, is obtained from feature extraction. Similarly each image in the database is represented with feature vector $f_{\mathrm{DB}_j} = (f_{\mathrm{DB}_{j1}}, f_{\mathrm{DB}_{j2}}, \ldots, f_{\mathrm{DB}_{jLg}});\quad j = 1, 2, \ldots, |\mathrm{DB}|$. The goal is to select the n best images that resemble the query image. This involves selection of n top matched images by measuring the distance between query image and images in the database $|\mathrm{DB}|$. In order to match the images, we use d_1 similarity

TABLE II
GROUPWISE PERFORMANCE OF VARIOUS METHODS IN TERMS OF ARP ON OASIS-MRI DATABASE

Method	Precision (%) (n=10)				
	Group 1	Group 2	Group 3	Group 4	Total
LBPu2_8_1	51.77	32.54	33.82	49.06	42.63
LBPu2_16_2	52.58	38.43	31.68	51.13	44.37
LBPu2_24_3	45.88	42.64	33.7	49.53	43.44
GLBPu2_8_1	54.43	37.94	26.51	46.03	42.42
GLBPu2_16_2	61.12	41.17	29.43	48.11	46.31
GLBPu2_24_3	72.01	31.37	32.36	47.83	47.69
DBWPu2_8_1	52.74	37.74	34.38	60	47.05
DBWPu2_16_2	57.74	34.7	30.78	66.69	48.71
DBWPu2_24_3	52.98	37.15	37.42	71.79	50.59
LMePu2_8_1	52.82	36.56	36.08	51.50	44.96
LMePu2_16_2	57.82	42.84	39.89	60.37	50.4
LMePu2_24_3	60.32	41.27	37.51	56.22	49.00
GLMePu2_8_1	66.12	44.90	43.38	68.30	56.34
GLMePu2_16_2	64.83	40.49	37.19	69.71	53.54
GLMePu2_24_3	60.08	40.78	38.62	68.49	52.54

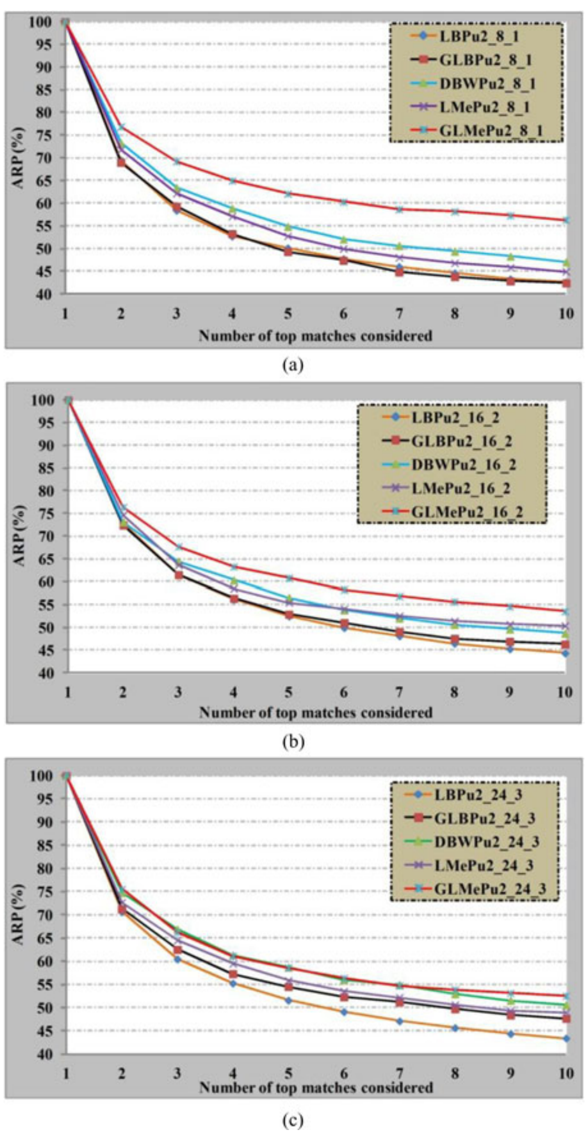

Fig. 7 Comparison of proposed method with other existing methods as function of number of top matches on OASIS database. (a) $P = 8$, $R = 1$; (b) $P = 16$, $R = 2$; and (c) $P = 24$, $R = 3$.

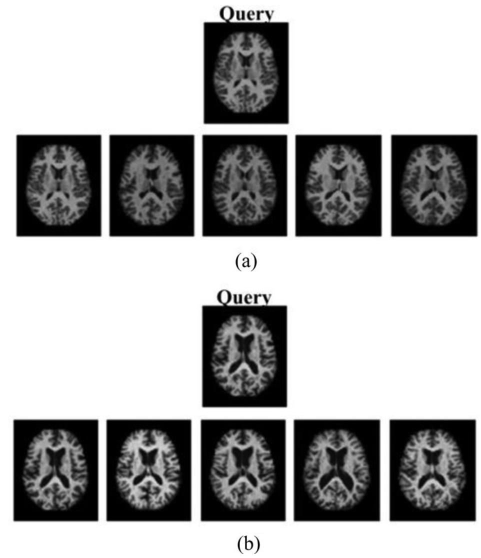

Fig. 8. Query results of LMeP on OASIS database.

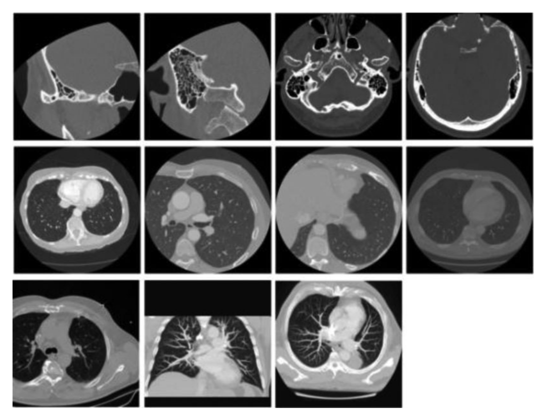

Fig. 9. Sample images from NEMA database (one image per category).

distance metric [32] computed using (16).

$$D(Q_i, \mathrm{DB}_{ji}) = \sum_{i=1}^{Lg} \left| \frac{f_{\mathrm{DB}_{ji}} - f_{Q_i}}{1 + f_{\mathrm{DB}_{ji}} + f_{Q_i}} \right| \tag{16}$$

where $f_{\mathrm{DB}_{ji}}$ is ith feature of jth image in the database $|\mathrm{DB}|$.

IV. EXPERIMENTAL RESULTS AND DISCUSSIONS

In order to analyze the performance of our algorithm for biomedical image retrieval three experiments were conducted on three different medical databases. Results obtained are discussed in the following sections.

Given below are the abbreviations used in the analysis of result:

LBP: *Local binary patterns [21]*
GLBP: *LBP with GT [21]*
DBWP: *Directional binary wavelet patterns [32]*
LMeP: *Local mesh patterns*
GLMeP: *LMeP with GT*

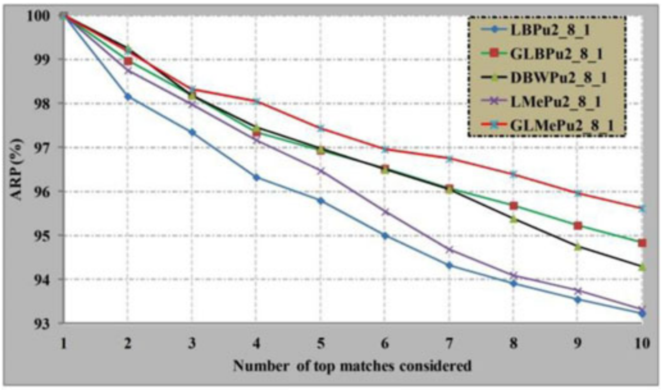

(a)

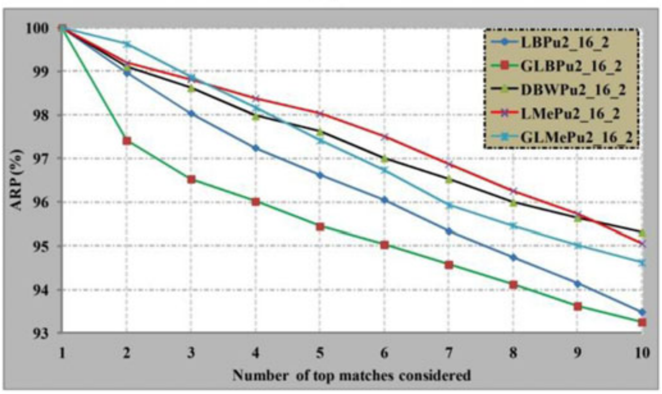

(b)

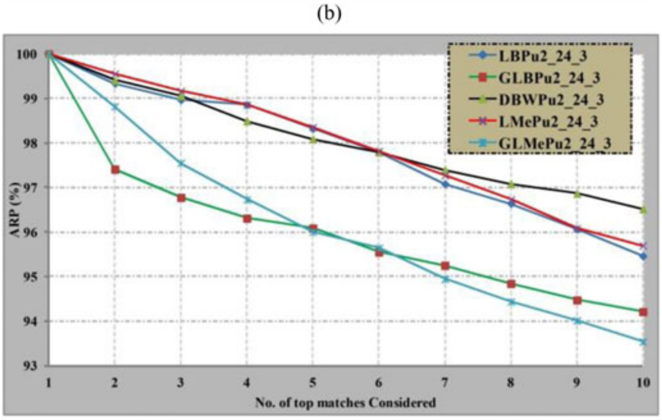

(c)

Fig. 10. Comparison of proposed method with other existing methods as function of number of top matches on NEMA-CT database. (a) $P = 8$, $R = 1$; (b) $P = 16$, $R = 2$; and (c) $P = 24$, $R = 3$.

INTH: *Intensity histogram [37]*

GLCM1: *Gray level cooccurrence matrix Type 1 (Autocorrelation) [37]]*

GLCM2: *Gray level cooccurrence Matrix Type 2 (Correlation) [37]*

GFB: *First four central moments of a Gaussian filter bank with four scales [37]*

LBP_P_Ru2: *LBP features collected from the uniform two pattern size (P,R); similar representation is applicable for all patterns.*

In all experiments, each image in the database is used as the query image. For each query, the system collects n database

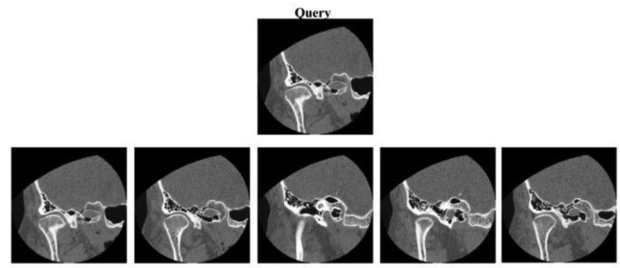

(a)

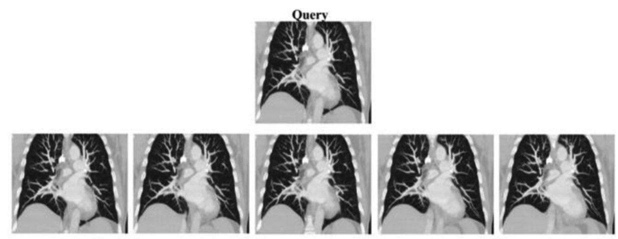

(b)

Fig. 11. Query results of LMeP on NEMA-CT database.

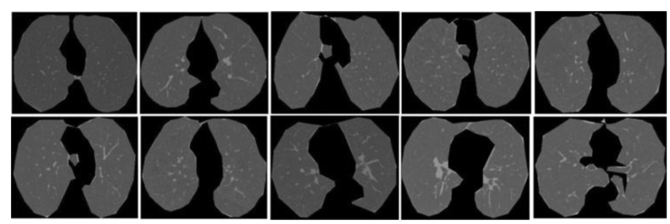

Fig. 12. Sample images from VIA/I-ELCAP—CT image database.

images $X = (x_1, x_2, \ldots, x_n)$, with the shortest image matching distance is given by (16). If x_i; $i = 1, 2, \ldots, n$ belong to the same category of the query image, we say the system has correctly matched the desired.

The average retrieval precision (ARP) and average retrieval rate (ARR) judge the performance of the proposed method those are calculated by (17)–(20).

For the query imageI_q, the precision (P) and recall (R) are defined as follows:

$$\text{Precision: } P(I_q) = \frac{\text{Number of Relevant Images Retrieved}}{\text{Total Number of Images Retrieved}} \tag{17}$$

$$\text{ARP} = \frac{1}{|\text{DB}|} \sum_{i=1}^{|\text{DB}|} P(I_i) \Bigg|_{n \le 10} \tag{18}$$

$$\text{Recall: } R(I_q) = \frac{\text{Number of Relevant Images Retrieved}}{\text{Total Number of Relevant Images in the Database}} \tag{19}$$

$$\text{ARR} = \frac{1}{|\text{DB}|} \sum_{i=1}^{|\text{DB}|} R(I_i) \Bigg|_{n \ge 10} \tag{20}$$

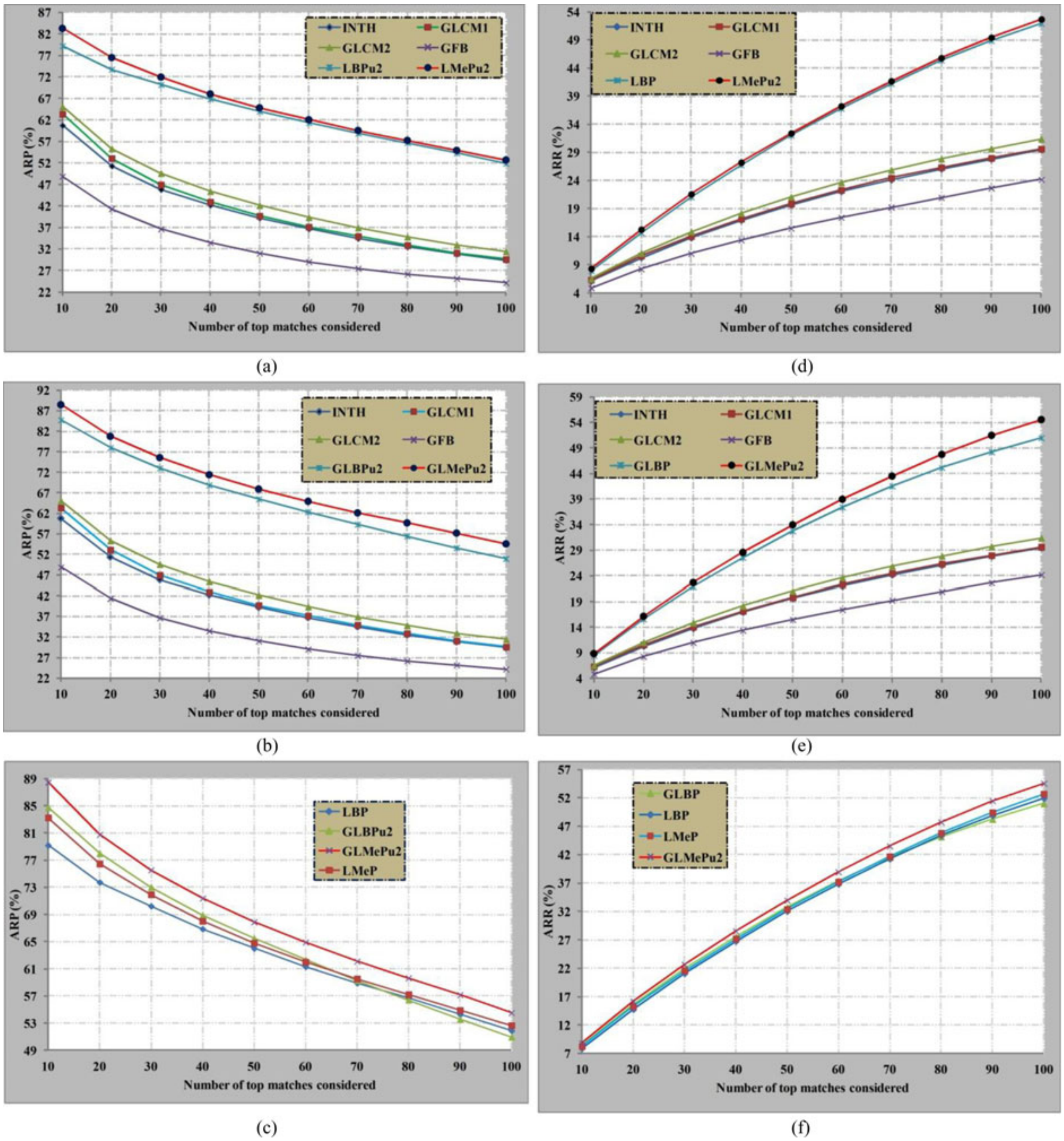

Fig. 13. Comparison of the LMeP/GLMeP with other existing spatial and transform domain methods in terms of: (a)–(c) ARP and (d)–(f) ARR on VIA/I-ELCAP–CT database.

A. Experiment 1

The Open Access Series of Imaging Studies (OASIS) [43] is a series of magnetic resonance imaging (MRI) dataset that is publicly available for study and analysis. This dataset consists of a cross-sectional collection of 421 subjects aged between 18 to 96 years. The MRI acquisition details are available in [43].

For image retrieval purpose, we grouped these 421 images into four categories (124, 102, 89, and 106 images) based on the shape of ventricular in the images. Fig. 6 depicts the sample images of OASIS database (one image from each category).

Table I illustrates the performance of GLMeP with different scales and $P/2$ directions on OASIS-MRI database. From Table I, it is clear that three scales and $P/2$ directions are outperforming the other scales of GLMeP.

Table II illustrates the group wise performance of various method with and without GT in terms of ARP on OASIS-MRI database. From Table II, the following inference is drawn for the performance of the proposed method with other methods in terms of ARP at $n = 10$.

1) ARP of LMePu2_8_1, LMePu2_16_2, and LMePu2_24_3 is more as compared to LBPu2_8_1, LBPu2_16_2, and LBPu2_24_3, respectively.

2) ARP of GLMePu2_8_1, GLMePu2_16_2, and GLMePu 2_24_3 is more as compared to LBPu2_8_1, LBPu2_16_2, GLBPu2_24_3, DBWPu2_8_1, DBWPu2_16_2, and DBWPu2_24_3, respectively on corresponding (P, R).

Fig. 7(a)–(c) shows the graphs depicting the retrieval performance of the proposed method and other existing methods as a function of number of top matches. From Fig. 7 and above observations, it is evident that the proposed method outperforms the other existing methods. Fig. 8 illustrates two query results of the proposed method by considering five top matches.

B. Experiment 2

The digital imaging and communications in medicine (DICOM) standard was created by the National Electrical Manufacturers Association (NEMA) [44] to aid the distribution and viewing of medical images, such as computer tomography (CT) scans, MRIs, and ultrasound. For this experiment, we have collected 681 CT scans of different parts of human body and these are grouped into 13 categories (45, 59, 46, 29, 36, 18, 37, 14, 139, 46, 143, 33, and 36 images). Fig. 9 depicts the sample images of NEMA database (one image from each category).

The retrieval performance of the proposed method (LMePu2/GLMePu2) and other existing methods (LBPu2/GLBPu2 and DBWPu2) as a function of number of top matches are given in Fig. 10(a)–(c). In this experiment, DBWPu2_16_2 and DBWP_24_3 are showing some similar performance to the proposed methods LMeP_16_2/ GLMeP_16_2 and LMeP_24_3/GLMeP_24_3, respectively, because binary wavelet patterns also extracts good directional information from this database. However, the feature vector length of DBWP is very high as compared to the proposed method (see in Section IV-D), which is an important requirement for online applications. From Fig. 10, it is concluded that the LMeP/GLMeP outperforms other existing methods. Fig. 11 illustrates two query results of the proposed method by considering five top matches on NEMA-CT database.

C. Experiment 3

Vision and image analysis (VIA) group and international early lung cancer action program (I-ELCAP) created a computer tomography (CT) dataset [45] for performance evaluation of different computer-aided detection systems. These images are in DICOM (digital imaging and communications in medicine) format. The CT scans were obtained in a single breath hold with a 1.25-mm slice thickness. The locations of nodules detected by the radiologist are also provided. For experiments, we have selected 10 scans. Each scan has 100 images with resolution 512 × 512. Furthermore, ROIs were annotated manually to construct the ROI CT image database. Fig. 12 depicts the sample images of VIA/I-ELCAP database (one image from each category).

Fig. 13 illustrates the retrieval performance of the proposed method (LMeP/GLMeP) and other existing methods (LBP/GLBP, INTH, GLCM1, GLCM2 and GFB) in terms of ARP and ARR. Fig. 14 illustrates the individual group performances of the LMeP/GLMeP and other existing methods in terms of precision and recall. From Figs. 13 and 14, it is clear that the proposed method (LMeP/GLMeP) outperforms other existing methods in terms of precision, recall, ARP, and ARR on VIA/I-ELCAP—CT database.

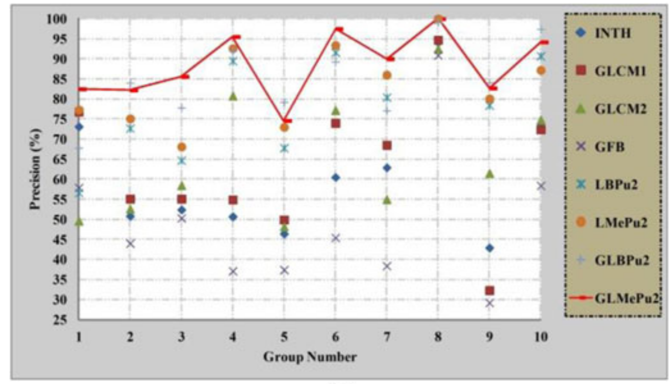

(a)

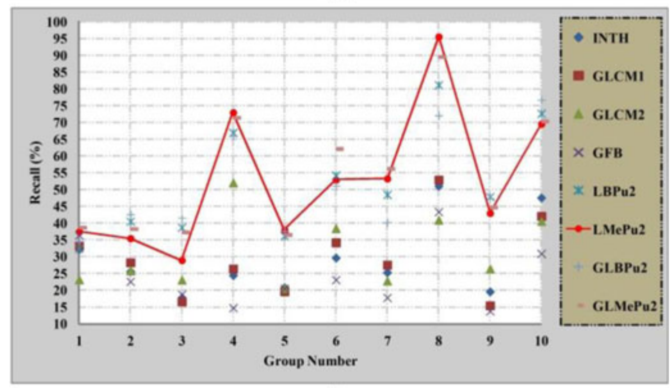

(b)

Fig. 14. GroupWise performance of LMeP/GLMeP and other existing methods in terms of : (a) precision and (b) recall on VIA/I-ELCAP—CT database.

TABLE III
FEATURE VECTOR LENGTH OF QUERY IMAGE USING VARIOUS METHODS

Method	Feature Vector Length	Execution Time (Seconds)
LBPu2_8_1	59	0.16
GLBPu2_8_1	12×59	0.97
DBWPu2_8_1	8×10×59	0.19
LMePu2_8_1	3×59	0.27
GLMePu2_8_1	3×3×59	0.85

D. Feature Vector Length V/S Performance

Table III shows the feature vector length and execution time for a given query image of size 256 × 256 using LBP, GLBP, DBWP, LMeP, and GLMeP. The experimentation is carried out on core2Duo computer with 2.66 GHz and all methods are implemented on the MATLAB 7.6 software. From the Table III, it is clear that the feature vector length of GLMeP is 8.8 times less as compared to DBWP and is outperforming the DBWP and other existing methods in terms of ARP and ARR on three different biomedical databases. The feature vector length and execution time of the LMeP is more as compared to the LBP, as it outperforms.

1) The LBP by 13.9%, 2.4%, and 9.2% in terms of ARP on OASIS-MRI, NEMA-CT and VIA/I-ELCAP-CT image databases, respectively.
2) The LBP by 3.12% in terms of ARR on VIA/I-ELCAP-CT image database.

V. Conclusion

In this paper, a new scheme, LMeP, is presented for biomedical image retrieval application. The LMeP is different from the existing LBP in a manner that it encodes the relationship among the surrounding neighbors, whereas LBP encodes the relationship between the reference pixel and its surrounding neighbors in an image. The performance of the proposed method is tested on three different biomedical databases. The result after being investigated show a significant improvement in terms of precision, recall, ARR, and ARP as compared to LBP and other existing methods on respective databases.

Acknowledgment

The authors would like to thank the associate editor and anonymous reviewers for insightful comments and helpful suggestions to improve the quality, which have been incorporated in this manuscript.

References

[1] G. Scott and C.-R. Shyu, "Knowledge-Driven multidimensional indexing structure for biomedical media database retrieval," *IEEE Trans. Inf. Tech. Biomed.*, vol. 11, no. 3, pp. 320–331, May 2007.

[2] H. C. Akakin and M. N. Gurcan, "Content-Based microscopic image retrieval system for multi-image queries," *IEEE Trans. Inf. Tech. Biomed.*, vol. 16, no. 4, pp. 758–769, Jul. 2012.

[3] A. Quddus and O. Basir, "Semantic image retrieval in magnetic resonance brain volumes," *IEEE Trans. Inf. Tech. Biomed.*, vol. 16, no. 3, pp. 348–355, May 2012.

[4] L. Zheng, A. W. Wetzel, J. Gilbertson, and M. J. Becich, "Design and analysis of a content-based pathology image retrieval system," *IEEE Trans. Inf. Tech. Biomed.*, vol. 7, no. 4, pp. 249–255, Dec. 2003.

[5] X. Xu, D.-J. Lee, S. Antani, and L. R. Long, "A Spine X-Ray image retrieval system using partial shape matching," *IEEE Trans. Inf. Tech. Biomed.*, vol. 12, no. 1, pp. 100–108, Jan. 2008.

[6] B. André, T. Vercauteren, A. M. Buchner, M. B. Wallace, and N. Ayache, "Learning semantic and visual similarity for endomicroscopy video retrieval," *IEEE Trans. Med. Imag.*, vol. 31, no. 6, pp. 1276–1288, Jun. 2012.

[7] Y. Rui and T. S. Huang, "Image retrieval: Current techniques, promising directions and open issues," *J. Vis. Commun. Image Represent.*, vol. 10, pp. 39–62, 1999.

[8] A. W. M. Smeulders, M. Worring, S. Santini, A. Gupta, and R. Jain, "Content-based image retrieval at the end of the early years," *IEEE Trans. Pattern Anal. Mach. Intell.*, vol. 22, no. 12, pp. 1349–1380, Dec. 2000.

[9] M. Kokare, B. N. Chatterji, and P. K. Biswas, "A survey on current content based image retrieval methods," *IETE J. Res.*, vol. 48, no. 3 and 4, pp. 261–271, 2002.

[10] Y. Liu, D. Zhang, G. Lu, and W.-Y. Ma, "A survey of content-based image retrieval with high-level semantics," *Pattern Recog.*, vol. 40, pp. 262–282, 2007.

[11] H. Muller, N. Michoux, D. Bandon, and A. Geisbuhler, "A review of content-based image retrieval systems in medical applications–Clinical benefits and future directions," *J. Med. Inf.*, vol. 73, no. 1, pp. 1–23, 2004.

[12] W. Cai, D. D. Feng, and R. Fulton, "Content-based retrieval of dynamic PET functional images," *IEEE Trans. Inf. Tech. Biomed.*, vol. 4, no. 2, pp. 152–158, Jun. 2000.

[13] M. M. Rahman, S. K. Antani, and G. R. Thoma, "A learning-based similarity fusion and filtering approach for biomedical image retrieval using SVM classification and relevance feedback," *IEEE Trans. Inf. Tech. Biomed.*, vol. 15, no. 4, pp. 640–646, Jul. 2011.

[14] R. Nakayama, H. Abe, J. Shiraishi, and K. Doil, "Evaluation of objective similarity measures for selecting similar images of mammographic lesions," *J. Digital Imag.*, vol. 24, no. 1, pp. 75–85, 2011.

[15] F. S. Zakeri, H. Behnam, and N. Ahmadinejad, "Classification of benign and malignant breast masses based on shape and texture features in sonography images," *J. Med. Syst.*, vol. 36, no. 3, pp. 1621–1627, 2012.

[16] L. Yang, Student, R. Jin, L. Mummert, R. Sukthankar, A. Goode, B. Zheng, S. C. H. Hoi, and M. Satyanarayanan, "A boosting framework for visuality-preserving distance metric learning and its application to medical image retrieval," *IEEE Trans. Pattern Anal. Mach. Intell.*, vol. 32, no. 1, pp. 33–44, Jan. 2010.

[17] G. Quellec, M. Lamard, G. Cazuguel, B. Cochener, and C. Roux, "Wavelet optimization for content-based image retrieval in medical databases," *J. Med. Image Anal.*, vol. 14, pp. 227–241, 2010.

[18] A. Traina, C. Castanon, and C. Traina Jr., "Multiwavemed: a system for medical image retrieval through wavelets transformations," in *Proc. 16th IEEE Symp. Comput.-Based Med. Syst.*, New York, NY, USA, 2003, pp. 150–155.

[19] J. C. Felipe, A. J. M. Traina, and C. Traina Jr., "Retrieval by content of medical images using texture for tissue identification," in *Proc. 16th IEEE Symp. Comput.-Based Med. Syst.*, New York, NY, USA, 2003, pp. 175–180.

[20] H. Muller, A. Rosset, J.-P. Vallet, and A. Geisbuhler, "Comparing feature sets for content-based image retrieval in a medical case database," in *Proc. SPIE Med. Imag., PACS Imag. Inf.*, San Diego, USA, 2004, pp. 99–109.

[21] T. Ojala, M. Pietikainen, and D. Harwood, "A comparative study of texture measures with classification based on feature distributions," *Pattern Recog.*, vol. 29, no. 1, pp. 51–59, 1996.

[22] T. Ojala, M. Pietikainen, and T. Maenpaa, "Multiresolution gray-scale and rotation invariant texture classification with local binary patterns," *IEEE Trans. Pattern Anal. Mach. Intell.*, vol. 24, no. 7, pp. 971–987, Jul. 2002.

[23] Z. Guo, L. Zhang, and D. Zhang, "Rotation invariant texture classification using LBP variance with global matching," *Pattern Recog.*, vol. 43, pp. 706–716, 2010.

[24] S. Liao, M. W. K. Law, and A. C. S. Chung, "Dominant local binary patterns for texture classification," *IEEE Tans. Image Proc.*, vol. 18, no. 5, pp. 1107–1118, May 2009.

[25] Z. Guo, L. Zhang, and D. Zhang, "A completed modeling of local binary pattern operator for texture classification," *IEEE Tans. Image Proc.*, vol. 19, no. 6, pp. 1657–1663, Jun. 2010.

[26] T. Ahonen, A. Hadid, and M. Pietikainen, "Face description with local binary patterns: Applications to face recognition," *IEEE Trans. Pattern Anal. Mach. Intell.*, vol. 28, no. 12, pp. 2037–2041, Dec. 2006.

[27] B. Zhang, Y. Gao, S. Zhao, and J. Liu, "Local derivative pattern versus local binary pattern: Face recognition with higher-order local pattern descriptor," *IEEE Trans. Image Process.*, vol. 19, no. 2, pp. 533–544, Feb. 2010.

[28] X. Tan and B. Triggs, "Enhanced local texture feature sets for face recognition under difficult lighting conditions," *IEEE Trans. Image Process.*, vol. 19, no. 6, pp. 1635–1650, Jun. 2010.

[29] J. Ning, L. Zhang, D. Zhang, and W. Chengke, "Robust object tracking using joint color-texture histogram," *Int. J. Pattern Recog. Artif. Intell.*, vol. 23, no. 7, pp. 1245–1263, 2009.

[30] S. Murala, R. P. Maheshwari, and R. Balasubramanian, "Local maximum edge binary patterns: A new descriptor for image retrieval and object tracking," *Signal Process.*, vol. 92, pp. 1467–1479, 2012.

[31] S. Murala, R. P. Maheshwari, and R. Balasubramanian, "Directional local extrema patterns: A new descriptor for content based image retrieval," *Int. J. Multimedia Inf. Retrieval*, vol. 1, pp. 191–203, 2012.

[32] S. Murala, R. P. Maheshwari, and R. Balasubramanian, "Directional binary wavelet patterns for biomedical image indexing and retrieval," *J. Med. Syst.*, vol. 36, pp. 2865–2879, 2012.

[33] V. Takala, T. Ahonen, and M. Pietikainen, "Block-based methods for image retrieval using local binary pat-terns," in *Proc. Scandinavian Conf. Image Anal.*, 2005, vol. 3450, pp. 882–891.

[34] C.-H. Yao and S.-Y. Chen, "Retrieval of translated, rotated and scaled color textures," *Pattern Recog.*, vol. 36, pp. 913–929, 2003.

[35] S. Peng, D. Kim, S. Lee, and M. Lim, "Texture feature extraction on uniformity estimation for local brightness and structure in chest CT images," *J. Compt. Biol. Med.*, vol. 40, pp. 931–942, 2010.

[36] D. Unay, A. Ekin, and R. S. Jasinschi, "Local structure-based region-of-interest retrieval in brain MR images," *IEEE Trans. Inf. Tech. Biomed.*, vol. 14, no. 4, pp. 897–903, Jul. 2010.

[37] L. Sørensen, S. B. Shaker, and M. de Bruijne, "Quantitative analysis of pulmonary emphysema using local binary patterns," *IEEE Trans. Med. Imag.*, vol. 29, no. 2, pp. 559–569, Feb. 2010.
[38] M. Heikkil, MattiPietikainen, and C. Schmid, "Description of interest regions with local binary patterns," *Pattern Recog.*, vol. 42, pp. 425–436, 2009.
[39] B. Li and M. Q.-H. Meng, "Tumor recognition in wireless capsule endoscopy images using textural features and SVM-Based feature selection," *IEEE Trans. Inf. Tech. Biomed.*, vol. 16, no. 3, pp. 323–329, May 2012.
[40] B. Li and M. Q.-H. Meng, "Computer-Aided detection of bleeding regions for capsule endoscopy images," *IEEE Trans. Biomed. Eng.*, vol. 56, no. 4, pp. 1032–1039, Apr. 2009.
[41] S. He, J. J. Soraghan, B. F. O'Reilly, and D. Xing, "Quantitative analysis of facial paralysis using local binary patterns in biomedical videos," *IEEE Trans. Biomed. Eng.*, vol. 56, no. 7, pp. 1864–1870, Jul. 2009.
[42] S. Murala, R. P. Maheshwari, and R. Balasubramanian, "Local tetra patterns: A new feature de-scriptor for content based image retrieval," *IEEE Trans. Image Process.*, vol. 21, no. 5, pp. 2874–2886, May 2012.
[43] D. S. Marcus, T. H. Wang, J. Parker, J. G. Csernansky, J. C. Morris, and R. L. Buckner, "Open access series of imaging studies (OASIS): Cross-sectional MRI data in young, middle aged, nondemented, and demented older adults," *J. Cogn. Neurosci.*, vol. 19, no. 9, pp. 1498–1507, 2007.
[44] NEMA-CT image database. (2012). [Online]. Available: ftp://medical.nema.org/medical/Dicom/Multiframe/
[45] VIA/I-ELCAP CT Lung Image Dataset, (2012). [Online] Available: http://www.via.cornell.edu/databases/lungdb.html

Subrahmanyam Murala was born in India in 1985. He received the M.Tech. and Ph.D. degrees from the Department of Electrical Engineering, Indian Institute of Technology Roorkee, Roorkee, India, in 2009 and 2012 respectively.

He is currently a Postdoctoral Researcher at Computer Vision and Sensing Systems Lab, Department of Electrical and Computer Engineering, University of Windsor, Windsor, ON, Canada.

His major research interests include image retrieval, medical imaging, face recognition, pattern recognition, and object tracking.

Q. M. Jonathan Wu (M'92–SM'09) received the Ph.D. degree in electrical engineering from the University of Wales, Swansea, U.K., in 1990.

He was with the National Research Council of Canada for ten years from 1995, where he became a Senior Research Officer and a Group Leader. He is currently a Professor with the Department of Electrical and Computer Engineering, University of Windsor, Windsor, ON, Canada. He has published more than 250 peer-reviewed papers in computer vision, image processing, intelligent systems, robotics, and integrated microsystems. His current research interests include 3-D computer vision, active video object tracking and extraction, interactive multimedia, sensor analysis and fusion, and visual sensor networks.

Dr. Wu holds the Tier 1 Canada Research Chair in Automotive Sensors and Information Systems. He is an Associate Editor for the IEEE TRANSACTIONS ON SYSTEMS, MAN, and CYBERNETICS PART A, and the *International Journal of Robotics and Automation*. He has served on technical program committees and international advisory committees for many prestigious conferences.